JAERI-M
6689

EXPERIMENTS WITH A RESISTIVE MODEL SHELL FOR TOKAMAK APPARATUS

August 1976

Taro SOMETANI* and Noboru FUJISAWA

日本原子力研究所
Japan Atomic Energy Research Institute

この報告書は，日本原子力研究所がJAERI-Mレポートとして，不定期に刊行している研究報告書です．入手，複製などのお問合わせは，日本原子力研究所技術情報部（茨城県那珂郡東海村）あて，お申しこしください．

JAERI-M reports, issued irregularly, describe the results of research works carried out in JAERI. Inquiries about the availability of reports and their reproduction should be addressed to Division of Technical Information, Japan Atomic Energy Research Institute, Tokai-mura, Naka-gun, Ibaraki-ken, Japan.

JAERI-M 6689

Experiments with a Resistive Model Shell for Tokamak Apparatus

Taro SOMETANI* and Noboru FUJISAWA

Division of Thermonuclear Fusion Research, Tokai, JAERI

(Received August 3, 1976)

The distribution of image current (shell current) in a resistive model shell has been measured. A plasma simulator is set in the shell; it is fed with a sinusoidal current of variable frequency. The distributions of shell current at different frequencies are obtained, following the Ampere's law, from signals of the magnetic probes located on internal and external surfaces of the shell. Intensity of the shell current increases as the simulator is displaced outward and the frequency is raised. Intensity of the shell current does not vary as a sinusoidal function of the poloidal angle of the shell. When frequency of the simulator current is raised sufficientry to make thickness of the shell equal to its skin depth, intensity of the shell current becomes independent of the frequency. The vertical magnetic field produced by the shell current is obtained from signals of the magnetic probes located on the simulator. Intensity of the measured field coincides with that of the vertical magnetic field calculated with the measured distribution of shell current. The current densities on internal and external surfaces of the ideal model shell are also measured.

---

* Department of Electrical Engineering, Faculty of Engineering, Shizuoka University, Hamamatsu.

JAERI－M 6689

トカマク装置の抵抗性シェルのモデル実験

日本原子力研究所東海研究所
核融合研究部
染谷太郎*・藤沢　登

（1976年8月3日受理）

トカマク装置の抵抗性シェルに誘起される電流を，モデルを用いて測定した。モデルシェル内に，プラズマ電流をシミュレートする導線を置き，その位置，そこに流す電流の周波数を種々変えて測定を行った。プラズマ電流シミュレータの大半径を大きくする，あるいはその電流の周波数を上げると，シェルに流れる電流は増加する。またシェルを流れる電流のポロイダル方向の分布は，余弦分布からややずれている。さらにシェルを流れる電流の作る垂直磁場の測定も行ったが，これは電流分布から計算によって求めたものと良く一致している。

* 静岡大学工学部

目　次　な　し

1. INTRODUCTION

In a Tokamak apparatus, an ideally conducting shell (an ideal shell) helps to keep a toroidal plasma in equilibrium [1]. When the plasma displaces, for example, outwards, the image curent in the outward part of the shell repels the plasma inwards, and at the same time, the image current in the inward part of the shell pulls the plasma inwards. The ideal shell itself can be considered as a feedback controlling or cybernetic means for control of the position of the toroidal plasma [2]. However, in a future fusion reactor, a bulk ideal shell made of copper or aluminum will not be used. This is because such materials of high electrical conductivity are apt to suffer damages by heat, neutrons, charged particles, and so on from the core of the reactor. If a shell is to be used in the fusion reactor, then it will be made of material free from various damages. In general, the electrical conductivity of such material is lower at least by one order of magnitude compared with that of the ideal shell. The shell must be a resistive shell.

On the other hand, various trials to substitute an external feedback control system for the ideal shell have been reported [3] and [4]. In some cases, the resistive shell is used together with the feedback control system in order to improve the control of the plasma position. In analyzing or designing the feedback control system, the distribution of the image current in the resistive shell (the shell current) must be known as one of current sources producing the vertical magnetic field for plasma equilibrium. The equilibrium of a toroidal plasma in a thin resistive shell or casing is analyzed under a simplified condition [5]. In a real apparatus, however, the distribution of the shell current will vary as the plasma displaces. The intensity and the phase of the vertical magnetic field produced by the shell current will depend on the typical time interval of the displacement of the plasma.

The object of the present work is to measure the distribution of the shell current. An inducing magnetic field is applied to the shell from a plasma simulator fed with a sinusoidal current of a variable frequency. Induced magnetic field on the internal and external surfaces of the shell, and on the simulator are measured with magnetic probes. The distribution of the shell current is

obtained from the signals of the magnetic probes in accordance with the Ampere's law.

2. ARRANGEMENT AND METHOD OF EXPERIMENT

The schematic diagram of the present experiment is shown in Fig.1. The main components of the experimental arrangement are as follows.

1) Model shell: A model shell made of aluminum has dimensions (thickness; 6 mm, major radius;180 mm, and inner minor radius;72 mm) 1/5 times as large as those of the JFT-2 apparatus. The model shell can be resistive or ideal as the frequency of the simulator current varies.

2) Magnetic probes: Three sets of small magnetic probes are prepared, each set having seven magnetic probes. The magnetic probes of one set are located on the internal surface of the shell. The magnetic probes of another set are located on the external surface of the shell. The magnetic probes of the other set are located on the plasma simulator. All the magnetic probes are arranged at regular intervals of the poloidal angle of the shell or the simulator. The magnetic probes of each set are numbered in numerals from 1 through 7. The 1-st magnetic probe (with numeral 1) is the innermost one, and the 7-th magnetic probe (with numeral 7), the outermost one. The magnetic probes located on the internal snd external surfaces of the shell form seven pairs. These pairs are used to measure the shell current. The magnetic probes located on the plasma simulator are used to measure the magnetic field produced by the shell current around the simulator. Each magnetic probe is 5 mm in diameter, and 5 mm in length.

3) Plasma simulator: A plasma simulator is made of 36 toroidal loops connected in series. The toroidal loops are arranged on a toroidal surface (with a minor radius of 25 mm) at regualr intervals of the poloidal angle of the toroidal surface. The simulator is intended for simulating a toroidal plasma with a surfacial current of uniform density. In order to simulate plasmas of different major radii, three simulators are prepared. The major radii of them are R_{min}=172.5 mm, R_{med}=180 mm, and R_{max}=187.5 mm, respectively.

4) Power amplifier: A power amplifier can feed a sinusoidal current of several amperes p.p. (peak-to-peak) to the simulator in a frequency range of 30 Hz $\sim$ 10 kHz. The simulator current is not always adjusted to a constant value through the frequency range, but the data presented

are reduced for the case of 1 A p.p. of the simulator current.
5) Probe amplifier: A probe amplifier is used to amplify the signals in the magnetic probes. The probe amplifier consists of three stages connected in cascade. Each stage includes an emitter follower, a usual amplifier, and a filter to suppress the internal noise in the stage. The collector current in each stage is restricted to within 1 mA to lower the level of the internal noise. The probe amplifier is contained in a steel box for the purpose of magnetic shielding.
6) Transient converter (Wave memory): A transient converter with two channels is used to record both the amplified signals of the magnetic probes and the simulator current. The phase differences between the magnetic fields at various positions and the simulator current are obtained from the forms of the recorded signals.

3. RESULT OF EXPERIMENT

The amplified signal of the magnetic probe is calibrated with a Helmholtz coil for each frequency of the simulator current. The calibrated signal of the k-th magnetic probe is written in the form of $B_k \cos(\omega t+\Phi_k)$. Besides the subscript k, additional subscriptive letters i, o, and p are used in order to distinguish quantities associated with the internal surface of the shell, the external surface of the shell, and the surface of the simulator, respectively. The quantity Φ_k is the phase difference between the simulator current and the amplified signal of the magnetic probe, and includes a phase α due to the magnetic probe and to the probe amplifier. The phase α can be known by measuring the magnetic field of the Helmholtz coil. However, it has been determined as follows. Consider the circulation of the Ampere's law along a circle passing through all the centers of the magnetic probes in each of the sets. In any case of the sets, the net ampere-turns through the circle is equal to that of the simulator. The total current in the shell is zero, because the shell is divided into four sections by air gaps. As the line integral for the circulation, we take a numerical expression according to the Simpson'e formula as follows:

$$\frac{h}{3}\tilde{\sum_k} B_k = \frac{h}{3}\{B_1+B_7+4(B_2+B_4+B_6)+2(B_3+B_5)\} \qquad (1)$$

where h is the pitch of integration. Referring to Fig.2, we have a relation

$$\alpha = \tan^{-1} \frac{\tilde{\Sigma}_k B_k \sin\Phi_k}{\tilde{\Sigma}_k B_k \cos\Phi_k} \qquad (2)$$

The phase α is determined for each of the sets of the magnetic probes, and for each frequency of the simulator current. Thus, the net phase difference ϕ_k between the simulator current and the magnetic field, measured at respective location, is equal to $\phi_k - \alpha$. In Figs. 3 ∿ 8, the magnetic fields on the internal and external surfaces of the shell are shown. In these figures, the magnetic field is presented as the value at t=0, i.e. as $B_k \cos \phi_k$. The thickness (6 mm) of the shell) (with an electrical conductivity about 1/3 times as large as that of copper) is equal to the skin depth of the shell at a frequency of 200 Hz. In Figs.3 ∿ 8, the intensity of the magnetic field exibits no substantial dependence on frequency at a frequency higher than 200 Hz.

Figures 9 ∿ 11 show how the distribution of the magnetic field on the internal surface of the shell varies as the frequency changes. As the frequency increases, the shell current reduces the unbalance (due to toroidal effect) of the magnetic pressures at large and small major radius locations. The equilibrating function of the shell becomes remarkable as the frequency increases, and as the simulator displaces outwards.

The distribution of the shell current is obtained from the signals of the pairs of the magnetic probes located on the internal and external surfaces of the shell. The density of the shell current is given as the value in amperes per unit length of the shell in its poloidal direction, in disregard of the thickness of the shell. The dimensions in the sectional view in Fig.12 are as follows: r_s=75 mm, r_i=68.5 mm, r_{si}=72 mm, r_{so}=78 mm, and r_o=81.5 mm. Referring to Figs.12 and 13, and using the Ampere's law, one can obtain

$$x_k = \sqrt{\gamma (B_{ik})^2 + B_{ok}^2 - 2\gamma B_{ok} B_{ik} \cos(\Phi_{ik} - \Phi_{ok})} \quad (\text{gauß}) \qquad (3)$$

$$\gamma = \frac{\gamma_i}{\gamma_o} = 0.84$$

as a quantity proportional to the density of the shell current. The amplitude j_{sk} and the phase ϕ_{sk} of the shell current are given by

$$j_{sk} = \frac{1}{\mu_o} \frac{r_o}{r_c} x_k = 86.5\ x_k \qquad (A/m) \tag{4}$$

and

$$\phi_{sk} = \Phi_{ok} - \alpha_k - \sin^{-1} \{ \frac{\gamma B_{ik}}{x_k} \sin(\Phi_{ik} - \Phi_{ok}) \} \tag{5}$$

respectively. Figures 14 ∿ 16 show the distribution of the shell current density at t=0. Figures 17 ∿ 19 show the phase of the shell current density as a function of frequency.

The vertical magnetic field produced by the shell current is obtained from the signals of the 1-st and the 7-th magnetic probes located on the simulator. The calibrated value of either of these signals are presented by $B'_{pk}\cos(\omega t+\phi_{pk})$ when the simulator is set in the shell, and by $B_{pk}\cos\omega t$ when the simulator is taken out of the shell. The amplitude of the vertical magnetic field produced by the shell current is expressed in the form of

$$B_{vk} = \sqrt{B_{pk}^2 + B'^2_{pk} - 2B_{pk}B'_{pk}\cos\phi_{pk}} \tag{6}$$

The phase difference ϕ_{vk} between the simulator current and the vertical magnetic field produced by it is given by

$$\phi_{vk} = \mp \sin^{-1}(\frac{B_{pk}}{B_{vk}} \sin\phi_{pk}). \tag{7}$$

The vertical magnetic field at the location of the 1-st probe is negative (downwards) when the poloidal field at this location is positive. Thus, the upper sign of Eq. (7) is for k=1, and the lower sign is for k=7. Figures 20 ∿ 22 show the plots of Eqs. (6) and (7) as functions of frequency. for each simulator. Figures 23 ∿ 25 show the vertical magnetic field produced by the shell current at t=0, $B_{vk}\cos\phi_{vk}$. This vertical field can be calculated with the measured values of $j_{sk}\cos\phi_{sk}$, according to a numerical formula

$$B_{vk} = \frac{2h}{3} \sum_k^{\infty} j_{sk}\cos\phi_{sk}\ f_{k,\ell} \tag{8}$$

where h is the pitch equal to the arcuate length between two adjacent pairs of the magnetic probes. The factor $f_{k,\ell}$ is the vertical magnetic field, at the ℓ-th field point, which is produced by an electric current ring of 1 A put at the k-th location in the shell. As the field points for the vertical magnetic field, the following locations are chosen: the

location of the 7-th probe on the minimum simulator, the location of the 1-st probe on the maximum simulator, and the centers of the cross-sections of all the simulators. Any of the other possible field points, such as the location of the 1-st probe on the minimum simulator, is so close to the location of one of the electric current rings used for calculating the factor $f_{k,\ell}$ that Eq. (8) can not be used accurately. The vertical magnetic fields calculated according to Eq. (8) are shown also in Figs.23 ∿ 25.

The current density on the internal and external surfaces of an ideal model shell can be obtained also from the signals of the magnetic probes on the simulator. If the frequency of the simulator current increases enough to make the skin depth of the shell much smaller than its thickness, the image current on the internal surface does not produce magnetic field outside the internal surface, and that on the external surface does not produce magnetic field inside the external surface [6] and [7]. The internal current density j_{ik} and the external current density j_{ok} are given

$$j_{ik} = \frac{1}{\mu_o} \frac{r_i}{r_{si}} B_{ik} = 83.2 B_{ik} \qquad \text{(A/m)} \qquad (9)$$

and

$$j_{ok} = \frac{1}{\mu_o} \frac{r_o}{r_{so}} B_{ok} = 75.7 B_{ok} \qquad \text{(A/m)} \qquad (10)$$

respectively. The distributions of the internal and the external current densities are shown in Figs.26 ∿ 28. The external current density j_o, in each case of all the simulators, exibits a common distribution. This common distribution is to produce no magnetic field inside the external surface of the shell. The vertical magnetic field produced by the external current density is calculated according to a numerical formula similar to Eq.(8). The calculated distribution of the vertical magnetic field produced by the external current density is plotted in Fig.29. In this figure, also the calculated distribution of the vertical magnetic field produced by the average current density $\bar{j}_o = 1/18 \sum_k j_{ok}$ is plotted for comparison.

4. CONCLUSION

1) The intensity of the shell current increases as the plasma

simulator displaces outwards, and as the frequency of the simulator current increases. The density does not vary in a simple sinusoidal function of the poloidal angle of the shell.

2) A resistive shell has an equilibrating function for a toroidal plasma as an ideal shell has. When the frequency of the shell current is raised sufficiently to make the thickness of the shell equal to its skin depth, i.e. to a frequency of about 200 Hz, the intensity of the shell current becomes substantially independent on frequency.

3) The vertical magnetic field produced by the shell current is obtained from the signals of the magnetic probes located on the simulator. The amplitude and the phase of this vertical field show dependency on frequency to a frequency of about 200 Hz. When the simulator current is not sinusoidal but of a general wave form, the shell current and the vertical magnetic field produced by it will be obtained from the amplitude and the phase of the sinusoidal response, by using the Fourier transform of the simulator current. The measured vertical magnetic field is coincident with the vertical magnetic field calculated with the meadured distribution of the shell current.

4) The current densities at the internal and external surfaces of the shell are measured at a frequency sufficiently high to make the shell ideal. The magnetic field calculated with the measured distribution of the external current density is very small inside the shell as is expected.

REFERENCES

[1] MOROZOV, A.I., SOLOV'EV, L.S., Reviews of Plasma Physics Vol.2 Consultant Bureau Press, New York (1966).

[2] ARTSIMOVICH, L.A., KARTASHEV, K.B., Soviet Physics Doklady 7 (1962) 919.

[3] ARTEMENKOV, L.I., GOLOVIN, I.N., KOZLOV, P.I., MELIKHOV, P.I., SHVINDT, N.N., BUTENKO, V.K., GUBAREV, V.F., KUKHTENKO, A.I., LADIKOVROYEV, YU.P., SAMOILENKO, YU.I., Nucl. Fusion 12 (1972) Suppl. 27.

[4] HUGILL, J., GIBSON, A., Nucl. Fusion 14 (1974) 611.

[5] MUKHOVATOV, V.S., SHAFRANOV, V.D., Nucl. Fusion 11 (1971) 605.

[6] SOMETANI, T., ITOH, S., Japan. J. appl. Phys. 11 (1972) 1181.

[7] SOMETANI, T., ITOH, S., HASEBE, K., Japan. J. appl. Phys. 15 (1976) 141.

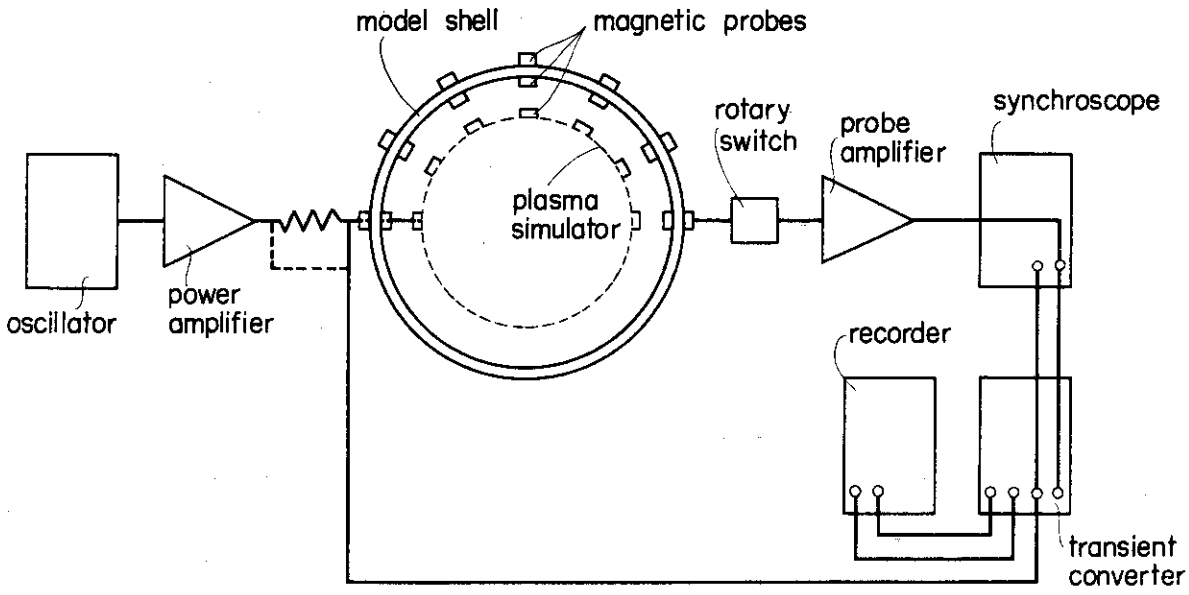

Fig.1: Schematic diagram of the experiment.

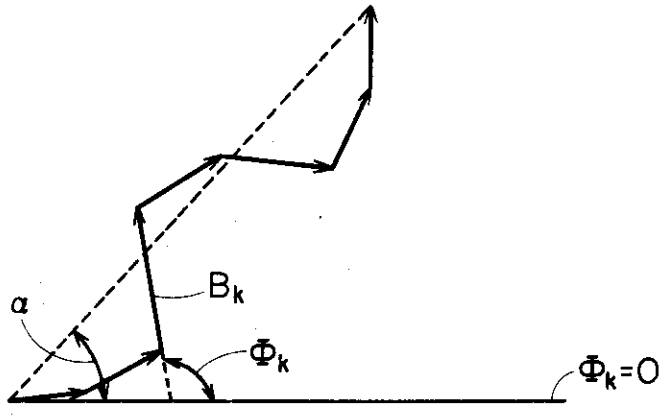

Fig.2: Vector diagram to determine the phase α due to a magnetic probe and to a probe amplifier.

Fig. 3

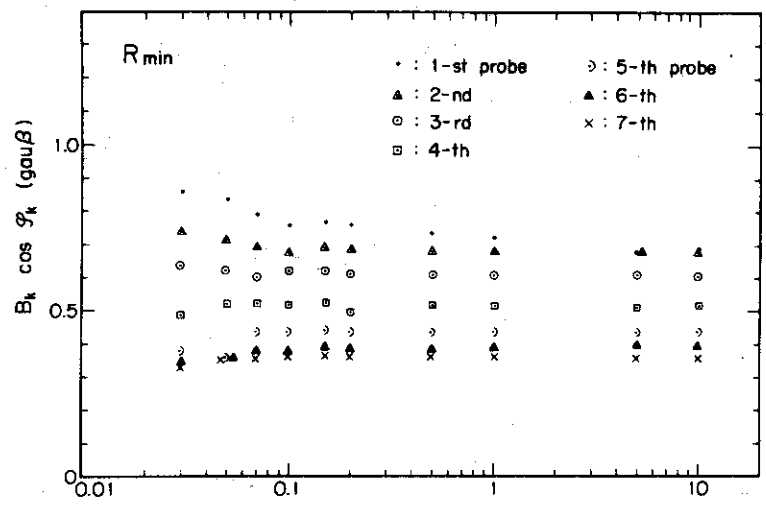

Fig. 4

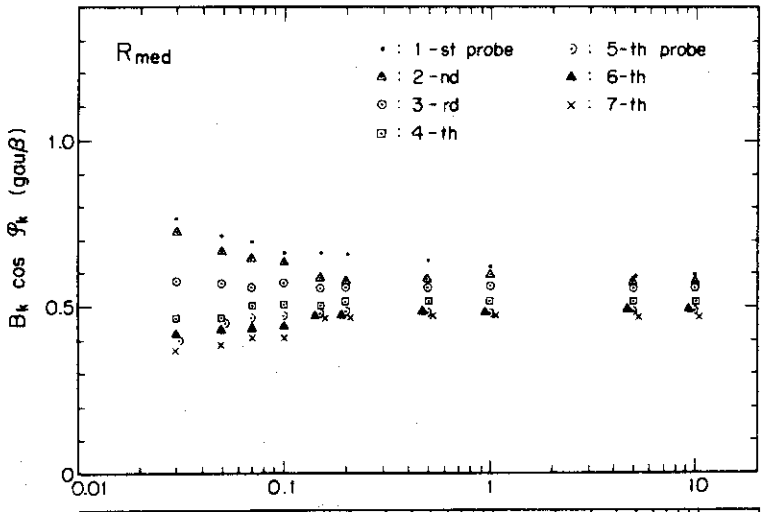

Fig. 5

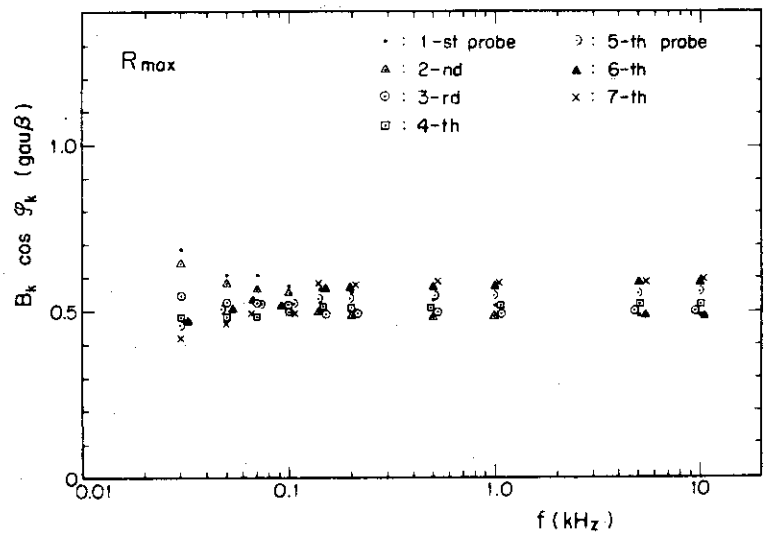

Figs.3∿5: Frequency dependence of the magnetic field on the internal surface of the shell containing the minimum simulator (Fig.3), the medium simulator (Fig.4), or the maximum simulator (Fig.5).

Fig. 6

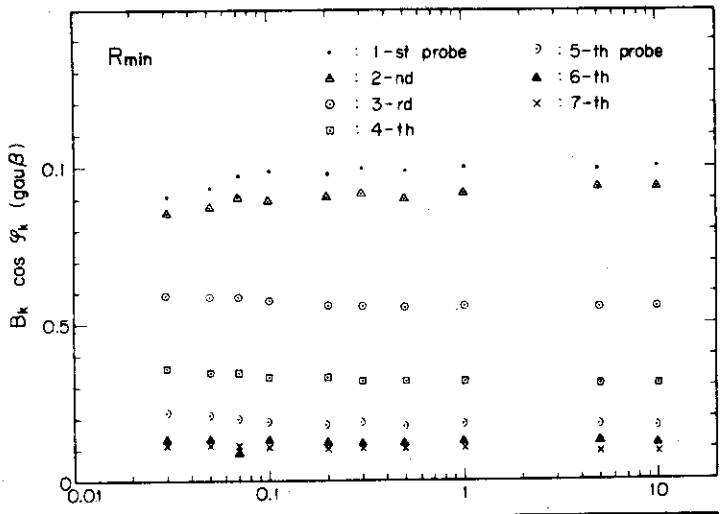

Fig. 7

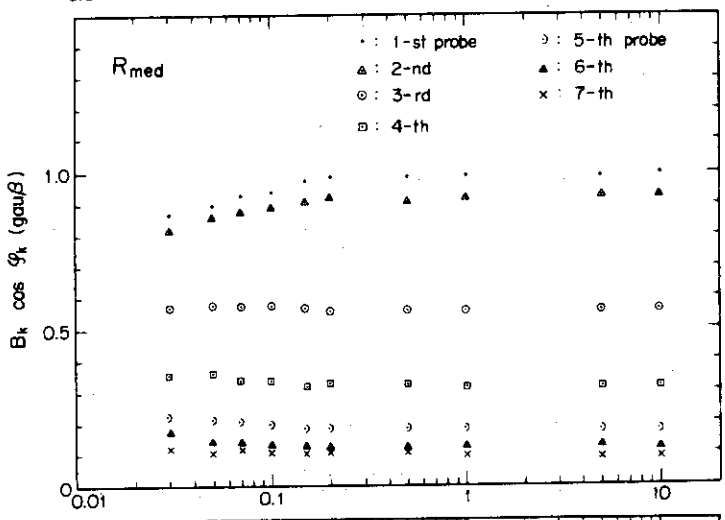

Fig. 8

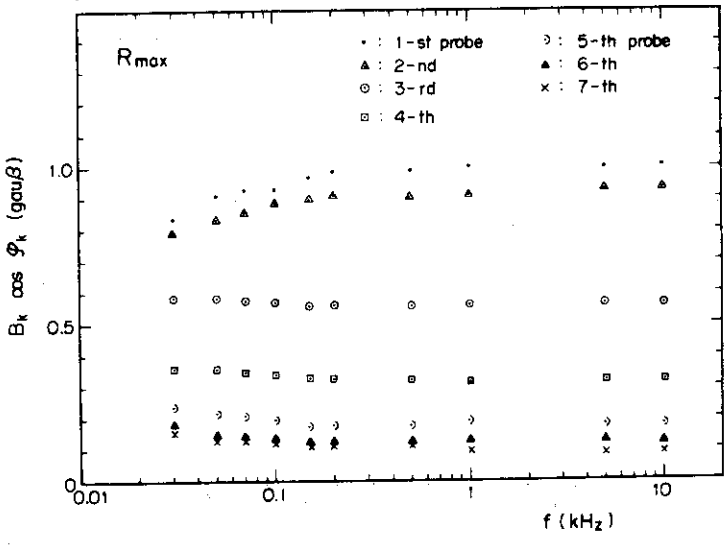

Figs.6∿8: Frequency dependence of the magnetic field on the external surface of the shell containing the minimum simulator (Fig.6), the medium simulator (Fig.7), or the maximum simulator (Fig.8).

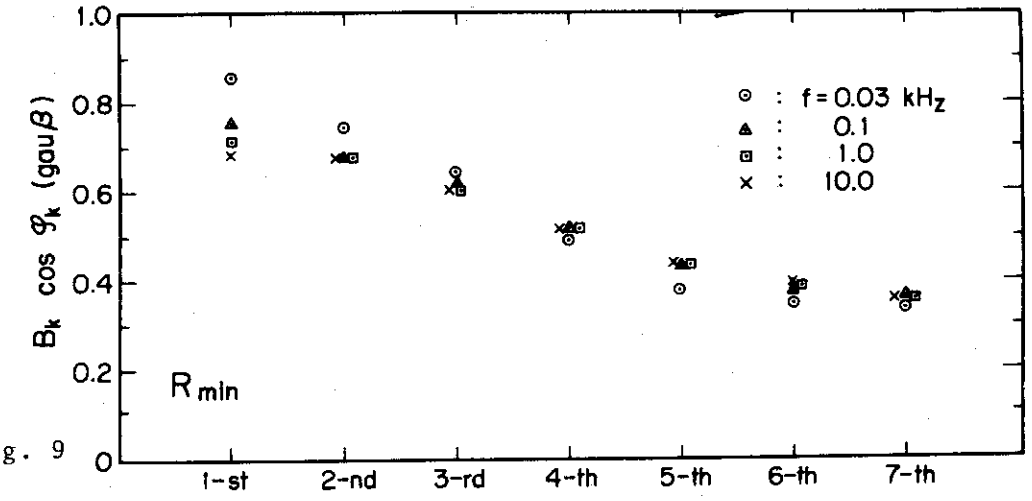

Fig. 9

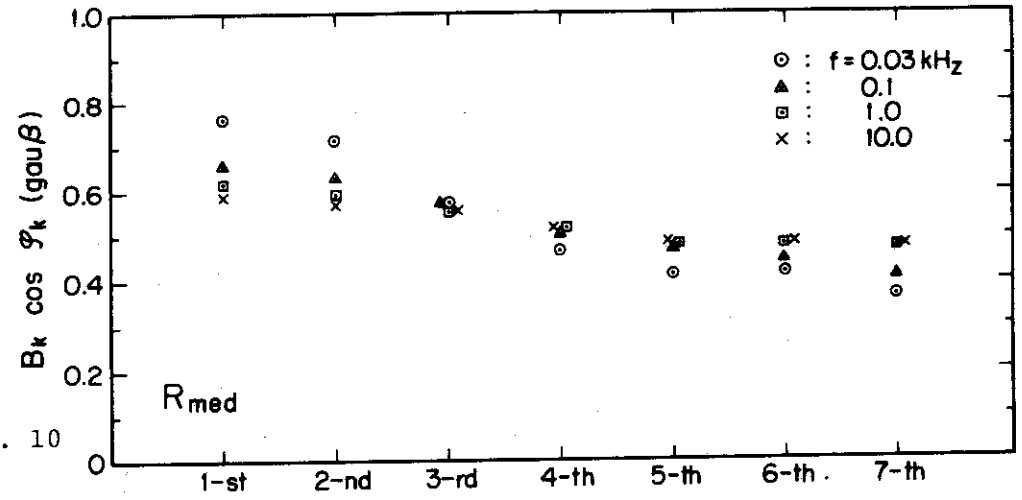

Fig. 10

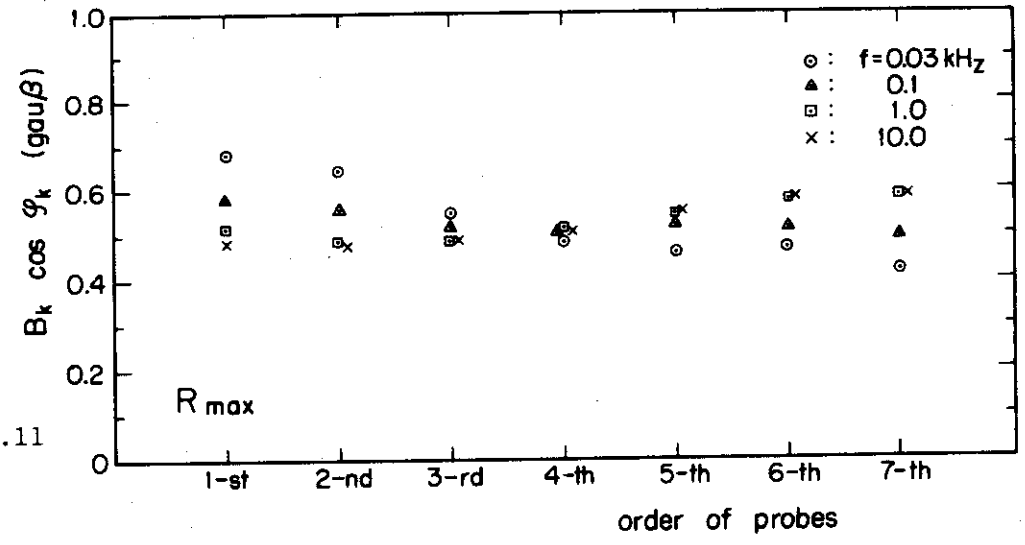

Fig.11

Figs.9∿11: Distribution of the magnetic field on the internal surface of the shell containing the minimum simulator (Fig.9), the medium simulator (Fig.10), or the maximum simulator (Fig.11).

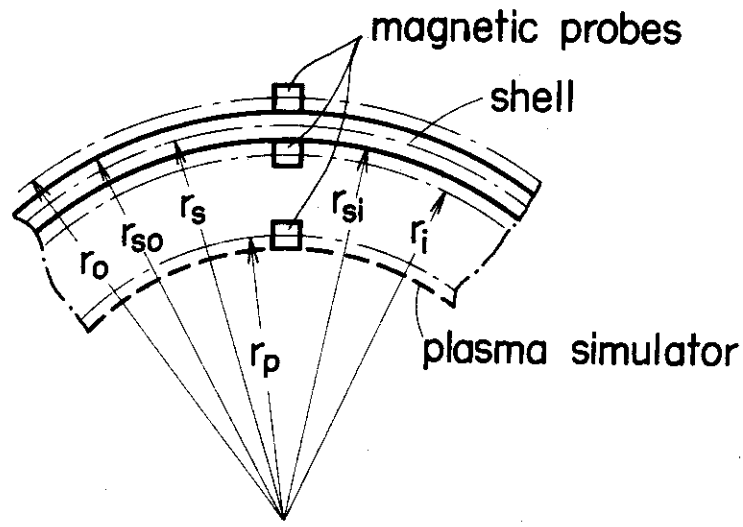

Fig.12: Sectional view of the shell and the simulator.

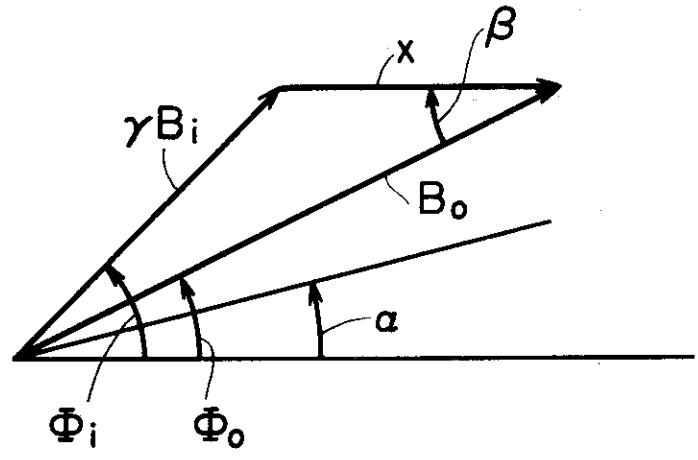

Fig.13: Vector diagram to obtain the shell current density.

Fig. 14

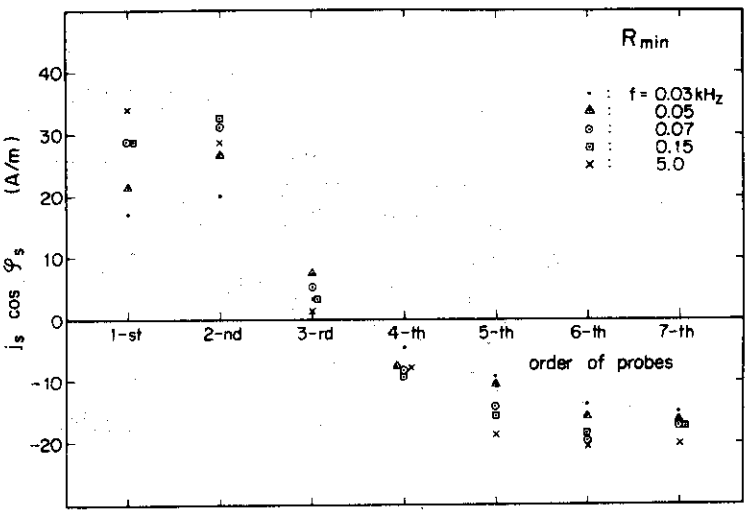

Fig. 15

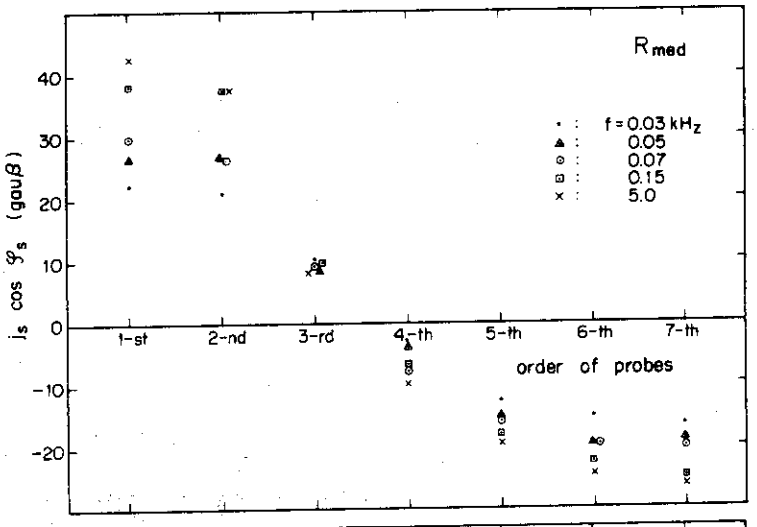

Fig. 16

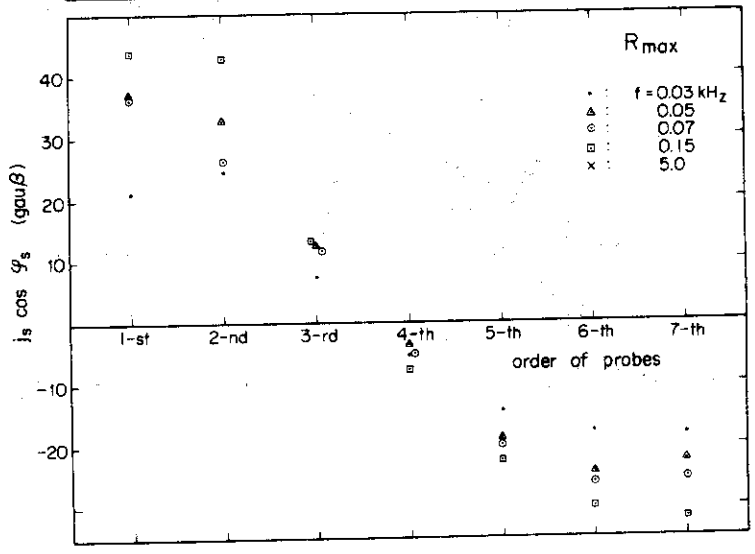

Figs.14 ∿ 16: Distribution of the shell current density at t=0 in the case of the minimum simulator (Fig.14), the medium simulator (Fig.15), or the maximum simulator (Fig.16).

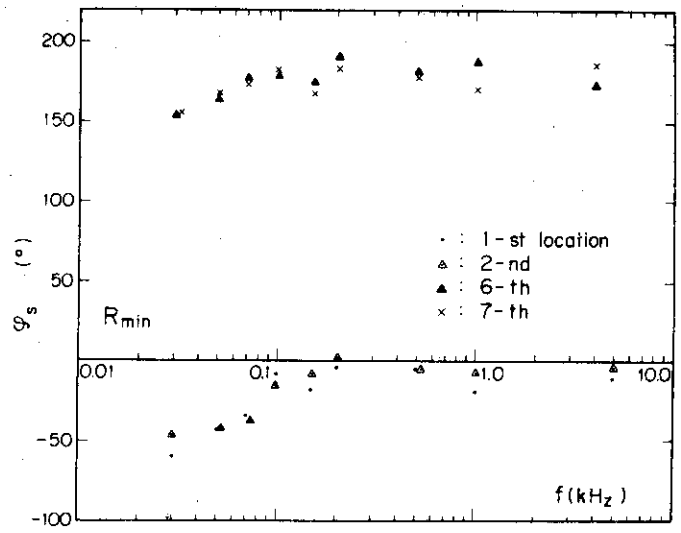

Fig. 17

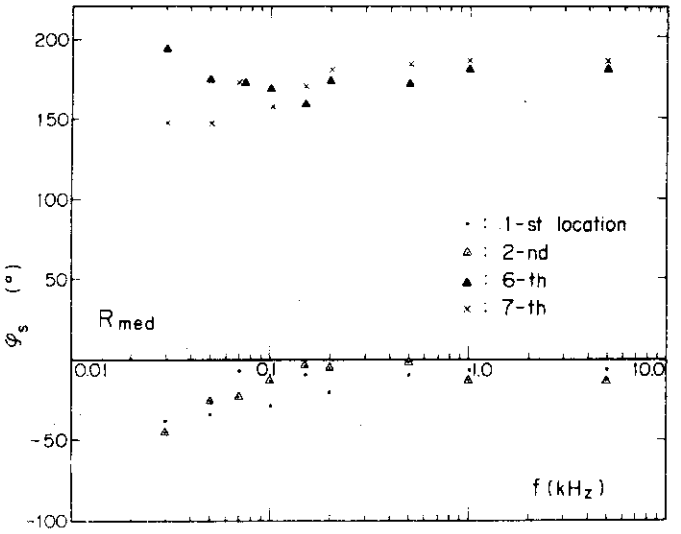

Fig. 18

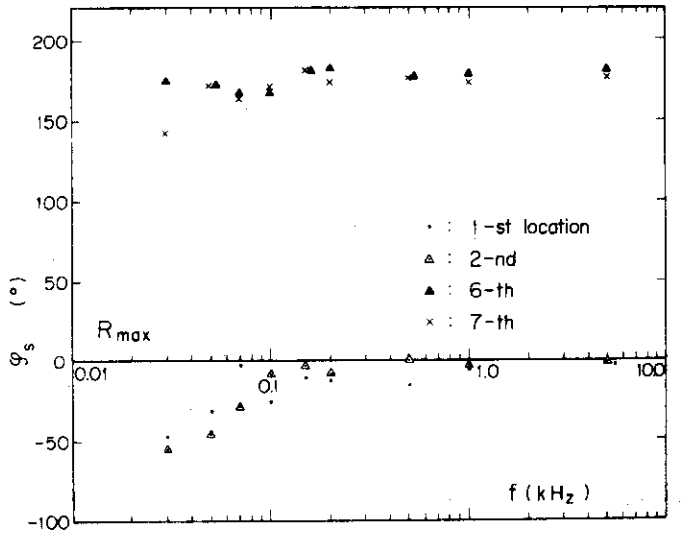

Fig. 19

Figs.17 ∿ 19: Frequency dependence of the phase of the shell current in the case of the minimum simulator (Fig.17), the medium simulator (Fig.18), or the maximum simulator (Fig.19).

Fig. 20

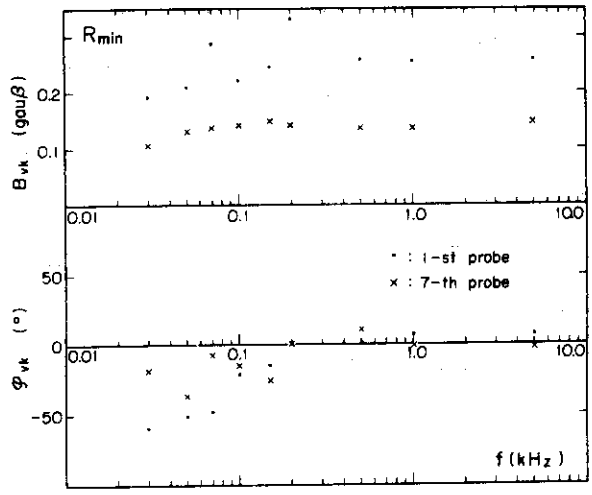

Fig. 21

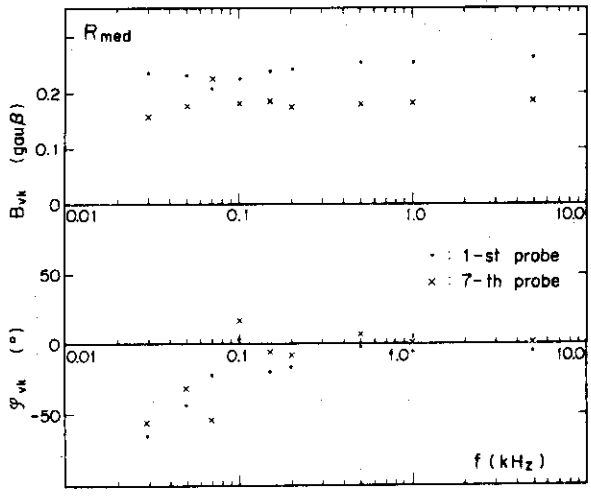

Fig. 22

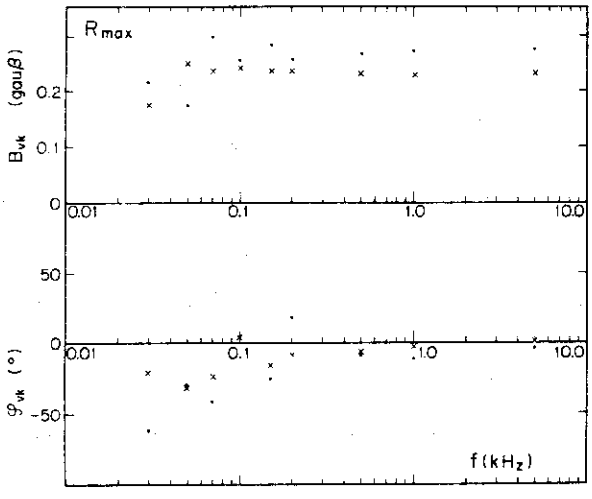

Fig.s20∿22: Frequency dependence of the amplitude and the phase of the vertical magnetic field produced by the shell current in the case of the minimum simulator (Fig.20), the medium simulator (Fig.21), or the maximum simultor (Fig.22).

Fig. 23

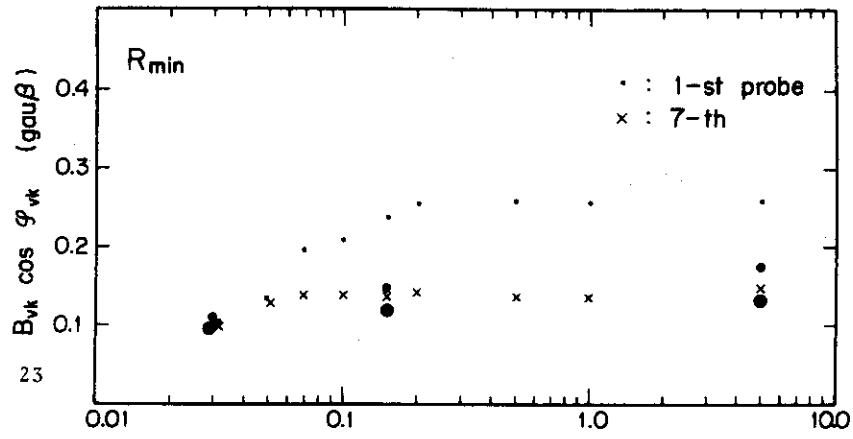

Fig. 24

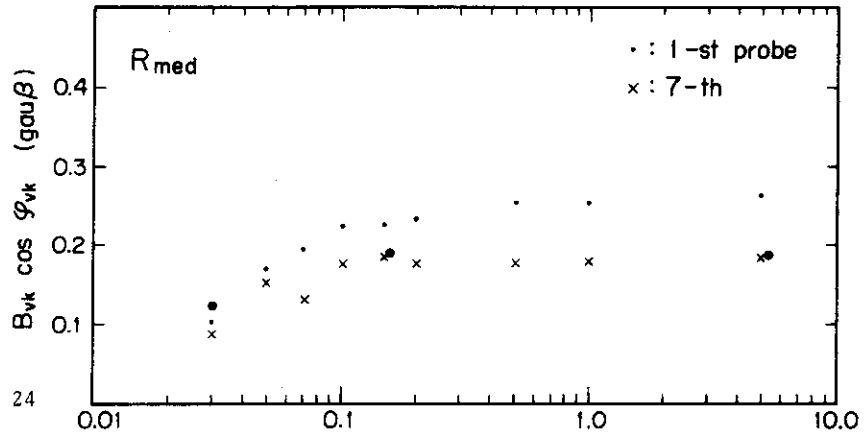

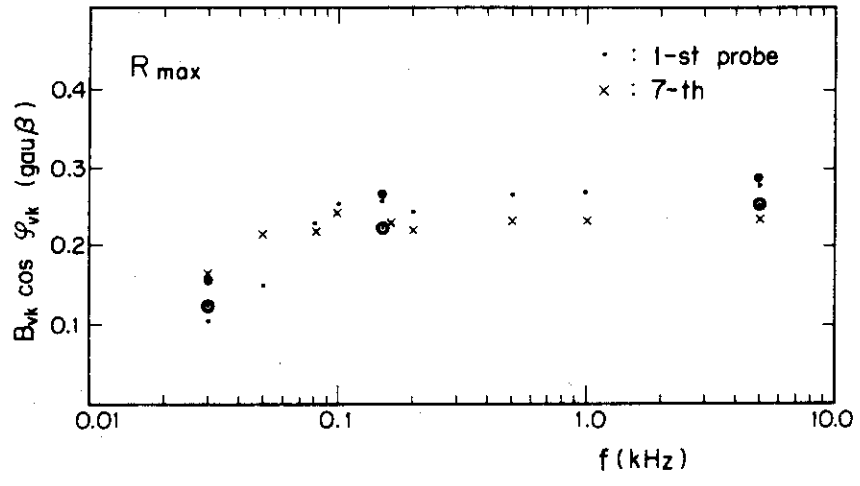

Figs.23∿25: Frequency dependence of the vertical magnetic field produced by the shell current at t=0, in the case of the minimum simulator (Fig.23), the medium simulator (Fig.24), or the maximum simulator (Fig.25). The vertical magnetic field calculated with the measured distribution of the shell current is also plotted for the following field points: the location of the 1-st probe on the simulator (◎), the location of the 7-th probe on the simulator (⊗), and the center of the cross-section of the simulator (●).

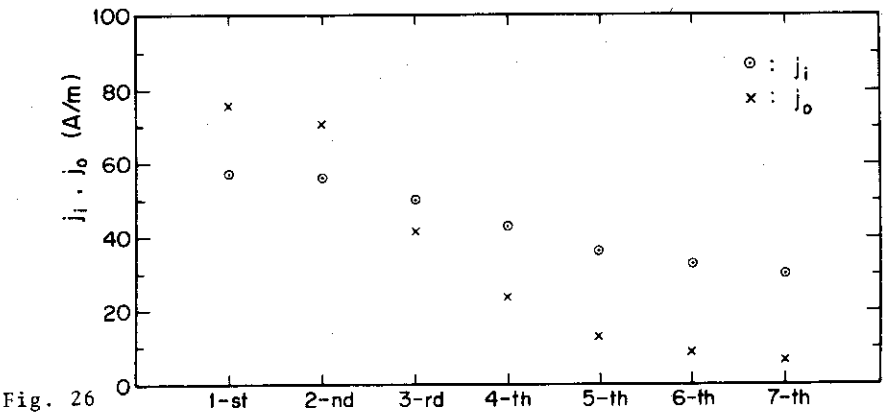

Fig. 26

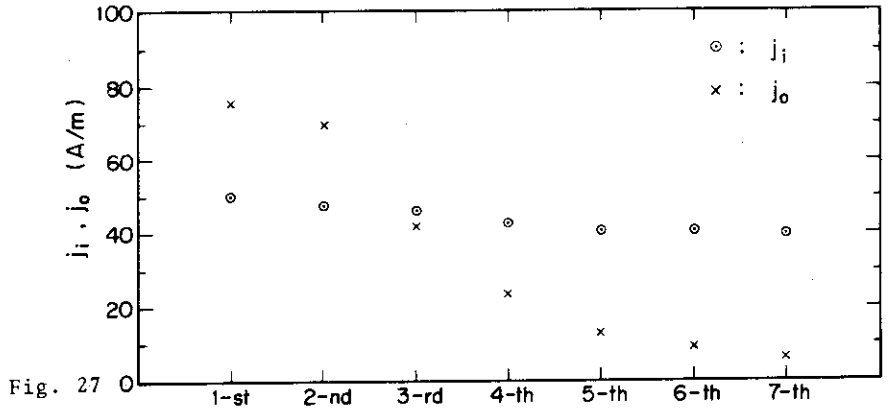

Fig. 27

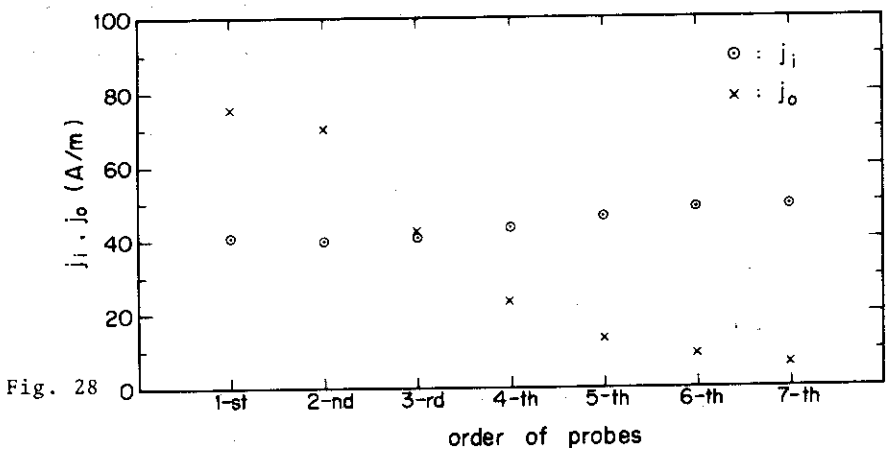

Fig. 28

Figs.26 ∿ 28: Distributions of the internal and the external current densities at a frequency of 10 kHz in the case of the minimum simulator (Fig.26), the medium simulator (Fig.27), or the maximum

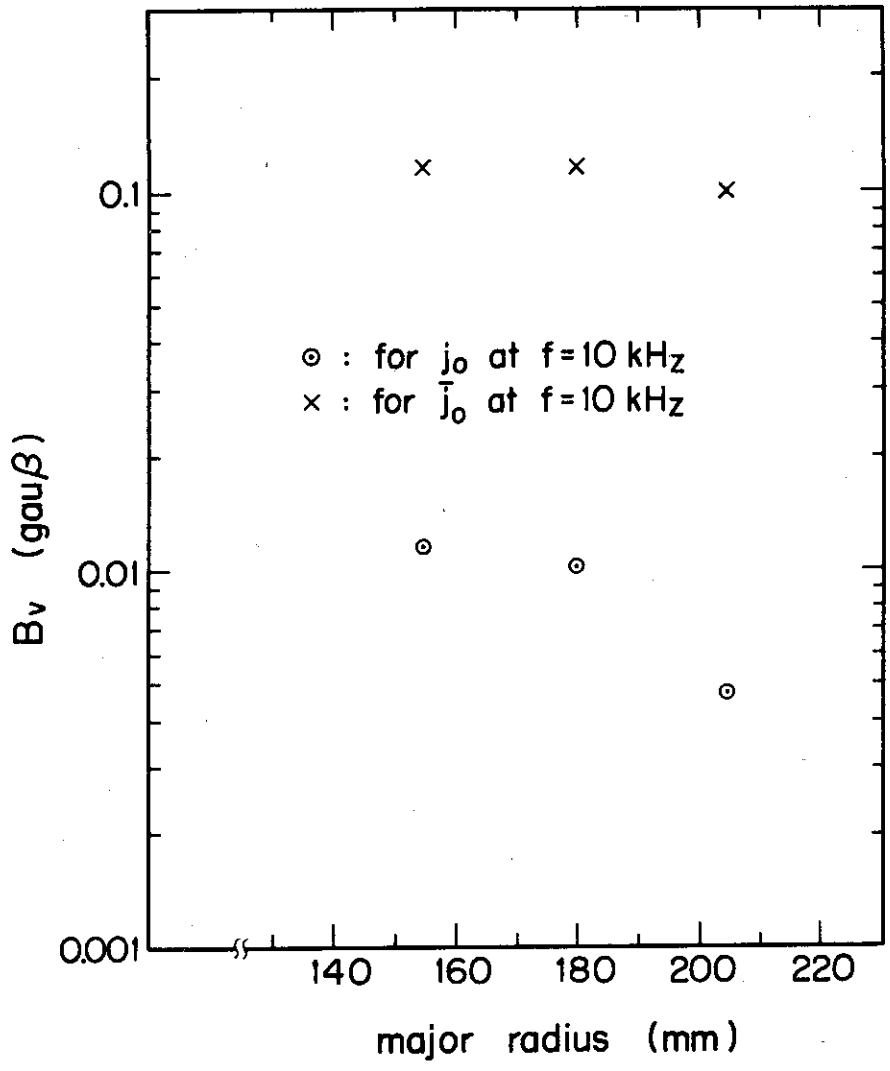

Fig.29: Calculated distributions of the vertical magnetic fields produced by the external current density (⊙), and the average external current density $j_o=1/18 \tilde{\sum_k} j_{ok}$ (×) at a frequency of 10 kHz.